



Final Report

CVD Synthesis, Structure Control and Characterizations of Nitrogen-Doped Single-Walled Carbon Nanotubes for Electrical and Mechanical Applications

Theerapol Thurakitseree

Final Report

CVD Synthesis, Structure Control and Characterizations of Nitrogen-Doped Single-Walled Carbon Nanotubes for Electrical and Mechanical Applications

Theerapol Thurakitseree Maejo University

บทคัดย่อ

รหัสโครงการ : TRG5780165

ชื่อโครงการ : การสังเคราะห์ วิเคราะห์และควบคุมโครงสร้างของคาร์บอนนาโนทิวบ์ผนังเดี่ยวที่เจือปนด้วย ในโตรเจนด้วยวิธีตกสะสมไอเคมีเพื่อการประยุกต์ใช้ในด้านไฟฟ้าและเชิงกล

ชื่อนักวิจัย : ธีรพล ธุระกิจเสรี มหาวิทยาลัยแม่โจ้

E-mail Address: zoonphysics@gmail.com, theerapol@mju.ac.th

ระยะเวลาโครงการ : 2 ปี

บทคัดย่อ: คาร์บอนนาโนทิวบ์ผนังเดี่ยวเป็นวัสดุระดับนาโนชนิดหนึ่งที่วิเศษและมีสมบัติที่น่าใจอย่างมาก ท่อนาโนคาร์บอนนี้เป็นที่รู้จักกันในแง่ของสมบัติในเชิงหนึ่งมิติ จากการทดลองและวิจัยทำให้เราทราบถึง สมบัติทางกายภาพ แสง และไฟฟ้าที่ยอดเยี่ยม ในปัจจุบันเราสามารถสังเคราะห์ท่อนาโนคาร์บอนที่มีคุณภาพ ในปริมาณมากในเชิงพาณิชย์ได้โดยใช้วัสดุเสริมร่วมกับตัวเร่งปฏิกิริยา การปรับปรุงสมบัติทางแสงและไฟฟ้า สามารถทำได้ได้หลายวิธี อาทิ การควบคุมโครงสร้าง หรือการเจือทางเคมี เนื่องจากสมบัติเฉพาะของท่อนา ้โนคาร์บอน มันจึงได้รับความสนใจเป็นอย่างมากในการประยุกต์ใช้ต่างๆ การปรับปรุงสมบัติทางแสงและ ไฟฟ้าระหว่างการสังเคราะห์ในกระบวนการตกสะสมไอเคมี (CVD) จึงเป็นเป้าหมายในระยะยาว ในการ สังเคราะห์ท่อนาโนคาร์บอนด้วยวิธีการทั่วไป เรามักจะไม่สามารถควบคุมโครงสร้างของท่อ (chirality) ได้มาก นัก อย่างไรก็ตาม เราสามารถควบคุมด้วยวิธีทางอ้อมได้โดยการควบคุมขนาดหรือช่วงของขนาดเส้นผ่าน ศูนย์กลางของท่อ ซึ่งเมื่อลดขนาดหรือช่วงขนาดลง จะส่งผลทำให้จำนวนโครงสร้างลดลงด้วยเหลือเพียงแต่ โครงสร้างที่ต้องการเพียงไม่กี่รูปแบบ อีกหนึ่งวิธีในการควบคุมสมบัติและโครงสร้างคือ การเจือด้วยธาตุอื่น ชึ่งจะส่งผลให้ท่อนาโนคาร์บอนสามารถเป็นได้ทั้งตัวนำหรือสารกึ่งตัวนำ ดังนั้นการจำกัดจำนวนของ โครงสร้างที่เป็นไปได้จึงได้รับความสนใจ ในการศึกษานี้ ผู้วิจัยทำการศึกษาผลกระทบของการเจือท่อนาโน คาร์บอนด้วยในโตรเจนต่อขนาดเส้นผ่านศูนย์กลาง จากการศึกษาพบว่า ขนาดเส้นผ่านศูนย์กลางสามารถทำ ได้โดยการเจือในโตรเจนระหว่างการสังเคราะห์ และพบว่าในกระบวนการ CVD นี้ ในโตรเจนจะเหนี่ยวนำให้ เกิดก๊าซไนโตรเจนขึ้นระหว่างปฏิกิริยาเคมี เมื่อทำการเปลี่ยนลำดับการให้แหล่งกำเนิดคาร์บอนที่มีชนิด ้ ต่างกัน ขนาดของท่อนาโนคาร์บอนสามารถเปลี่ยนแปลงได้ มากไปกว่านี้ผู้วิจัยยังได้ทำการศึกษารอยต่อ ระหว่างท่อที่มีขนาดต่างกันโดยวิธีการติดตามการย้ายผ่านของก๊าซไนโตรเจนระหว่างท่อ และการนำท่อนาโน คาร์บอนไปประยุกต์ใช้ในการเปลี่ยนพลังงานแลงอาทิตย์ให้เป็นพลังงานไฟฟ้าอีกด้วย

คำหลัก: คาร์บอนนาโนทิวบ์ผนังเดี่ยว การเจือด้วยในโตรเจน การควบคุมขนาดเส้นผ่านศูนย์กลาง การลด ขนาดเส้นผ่านศูนย์กลาง การห่อหุ้มก๊าซในโนโตรเจน

Abstract

Project Code: TRG5780165

Project Title: CVD Synthesis, Structure Control and Characterizations of Nitrogen-Doped Single-

Walled Carbon Nanotubes for Electrical and Mechanical Applications

Investigator: Theerapol Thurakitseree, Maejo University

E-mail Address: zoonphysics@gmail.com, theerapol@mju.ac.th

Project Period: 2 years

Abstract: Single-walled carbon (SWNT) has been well known as one of the wonderful nanomaterials, which has very interesting properties. It has been recognized as special onedimensional material fruitful with many promising properties. The experimental and theoretical studies have revealed its great physical, optical, and electrical properties. By utilizing catalyst support, mass production processes on SWNT synthesis have been commercialized, which provide good quality SWNTs for the next step of applications. Modifying electrical and optical properties of SWNTs has been obtained by many methods such as structure controlling, or chemical doping. Because of their intrinsic electrical property, those nanotubes have been given an emphasis on many applications. Tuning of electrical and optical properties of SWNTs during synthesis is a long standing goal in the chemical vapor deposition (CVD) synthesis of SWNTs. The direct synthesized SWNTs by conventional methods are inherently devoid of chirality control. Still, the electronic structures may be controlled indirectly by narrowing the diameter range to confine only the desired chiralities. By doping, SWNT properties can also be modified to be either metallic or semiconducting, depending on desired applications. Confinement of number of possible chirality, as well as, doping effect have consequently drawn intensively attention. In this study, the influence of nitrogen (N) doping on SWNT diameter structure was studied. It was found that nanotube diameter could be reduced by introducing N during synthesis process. By introducing N during CVD synthesis, N₂ molecules could be produced as by-product of chemical process. Upon switching feedstock introduction, SWNTs with different diameters could be obtained. The interface connection between tube-to-tube was investigated by tracing the migration of N₂ along the tube. Furthermore, the application of SWNTs on photovoltaic devices was also demonstrated.

Keywords: Carbon nanotubes, nitrogen doping, diameter control, diameter reduction, encapsulated nitrogen

1. Executive summary

The ability to tune the electrical and optical properties of single-walled carbon nanotubes (SWNTs) is a long-standing goal of SWNT synthesis. The properties of SWNTs are strongly dependent on their structure, and typically become more enhanced as the nanotube diameter decreases. As a result, chirality and diameter control particularly during synthesis offers a great potential for tuning the properties of nanotubes. Conventional methods generally provide nanotubes inherently devoid of chirality control. However, their electronic properties may be controlled indirectly by narrowing the diameter range to confine the number of possible chiralities. It is widely accepted that the nanotube diameter is largely determined by the size of the catalyst nanoparticle, and this size relationship has been thoroughly studied [1-9]. Because of this relationship, there have been many attempts to reduce the SWNT diameter by reducing the catalyst particle size. SWNTs with diameters in the range of 0.6-1.1 nm have been synthesized by impregnating SiO₂ particles with Co/Mo [1, 5, 10]. A similar selectivity has been obtained using Co/Fe [10, 11], Fe/MgO [12], and Co incorporated into MCM-411 [13]. These methods, however, require the use of powder and/or mesoporous material. Separating the SWNTs from the support requires significant post-processing, which can alter the nanotube properties. The direct control growth of SWNTs is, therefore, necessary for good quality and desired property of nanotubes.

Another possible way to control nanotube electrical property is by doping approach, e.g. direct post-treatment by chemical doping to modify charge transfer state [14–16]. The doping process can also be performed during growth process by introducing any carbon feedstocks containing desired dopants which introduce heteratoms into carbon lattice, while nanotubes are growing [17–19]. This process can be, therefore, performed in one step without any post-treatments. One of popular dopant is nitrogen, because it can provide either p-type or n-type, depending on its configurations with sp^2 C network. Pristine SWNTs generally behave as p-type material due to oxygen adsorption from atmospheric surrounding [20] in which oxygen take out electrons from carbon left only positive charge behind. Consequently, one of the most promising approaches of this N doping has been focused on producing a certain type of N configuration, which provide n-type characteristic or similar characteristic.

Synthesis of N-doped carbon nanotubes have been studied by many different synthesis processes [21–30]. While carbon nanotubes are being synthesizing, N can either leave the system or incorporate into a network of sp^2 carbon structure as pyridic, substitutional, or pyrrolic sites. It has been suggested that N-doped carbon nanotubes are in general contributed as bamboo shape by pyrrolic contribution [29] with minority of substitutional, and pyrrolic structures. The content of N incorporated in carbon nanotube walls is dependent of the solubility of N in the catalyst at growth

temperature [22]. Although this N content is proportional to N-containing feedstock concentration, most of N do not contribute in nanotube formation [24, 30].

While N doping seems to induce more defective than pristine undoped carbon nanotubes [17], N incorporation causes the diameter change. As N is incorporated or doped during growth process, tube diameter seems to be changed in the presence of more N source but the reason for constrained N content remains unclear. An slight increasing in the mean SWNT diameters from 1.6 to 1.67 nm has been previously shown by just introducing 500 ppm of ammonia with carbon feedstock [31]. It should be noted that ammonia (NH₃) can also act as etching agent for carbon nanotubes or nanofibers [32]. It is in this case plausible that ammonia may selectively etch away small-diameter SWNTs presented in the sample. Contrarily, a mean diameter tends to be reduced when feedstock used contains N radical. A reduction in diameter was found in N-doped SWNTs when acetonitrile concentration in ethanol is increased with the maximum N content of $\sim 1.5\pm 0.02$ at.% [33]. Similar work has also been reported on the same acetonitrile feedstock [108]. Ibrahim and co-workers [34] found a significantly change in nanotube mean diameter from 1.8 to 0.86 nm when acetonitrile mixtures were 0 and 100%. The N content was in this case ~2 at.% in maximum. As the SWNT diameter decreases, the energy formation seems to favor pyridinic-divacancy configuration rather than forming substitutional N site to lower the energy formation [35], while substitutional N configuration seems to be more favorable in graphene [36, 37]. Further studies on N configurationcontrolled process consequently need to be deserved to identify dopant configuration and electronic property in carbon nanotubes.

In this study, N-doped carbon nanotubes would be synthesized by chemical vapor deposition method (CVD) using pure ethanol and acetonitrile-mixed ethanol feedstocks as carbon source, while acetonitrile would be supplied as N source, which is supposed to produce a much small diameter nanotubes with nearly homogeneous properties. The aim of this doping research is, therefore, to be able to control the intrinsic property N-doping configuration during synthesis along with structure control of SWNT. The influence of N doping on SWNT diameter structure was studied. By switching feedstock introduction, SWNTs with different diameters could be obtained. The interface connection of different nanotubes on a double-layered vertically aligned SWNT array by tracing the migration of the molecules along the nanotubes has been demonstrated. By employing acetonitrile mixture as carbon/nitrogen feedstock, N₂ molecules could be produced and trapped inside the nanotube host. The ability to change feedstocks from ethanol to acetonitrile mixture during the CVD process is facile to synthesize a double-layered SWNT array. Using this approach we are able to synthesize two different SWNTs with and without encapsulated N₂ molecules at the bottom and the top layers of an array, respectively. As the carbon feedstock was switched, SWNTs undergo a transition from large to small diameters. With the combination of Raman spectroscopy and photoemission, the signature

of N_2 molecules present at the top of the top layer implies the N_2 migration across the interface boundary of diameter controlled layers of VA-SWNT arrays. The relative atomic N concentration of N_2 at the top layer is found to be approximately 1/4 of the original capacity of 0.3 at.% in pristine SWNTs synthesized from only acetonitrile mixture. Our findings prove a reasonable fraction of continuous intramolecular junctions in bulk scale SWNTs. Additionally, the application of SWNTs on photovoltaic devices was also demonstrated. A simple fabrication process of heterojunction solar cells from SWNTs and n-type silicon wafer are presented. SWNTs with nanotube mean diameter of about 1.1 nm were synthesized from alcohol-catalytic CVD, and were made into a film with transmittance of 70% by vacuum filtration. The patterned silicon substrate was prepared by a simple wet-etching process with hydrofuric acid utilizing a hand-made physical mask. The nanotube film was transferred onto the patterned silicon substrate. Power-conversion efficiency value of 4.3% with fill factor of 0.67 can be achieved.

2. Objective

- 1. To synthesize and narrow chirality distribution of single-walled carbon nanotubes (SWNTs) in order to obtain homogenous properties.
- 2. To investigates the influence of nitrogen doping on SWNT electrical properties.
- 3. To achieve large scale synthesis of SWNTs for applications.

3. Research methodology

3.1) Synthesis of N-doped SWNT and double-layered growth

The double-layered growth of VA-SWNT arrays were grown on silicon substrate by no-flow CVD [8]. Cobalt (Co) and molybdenum (Mo) acetate prepared by a liquid-dip coating process were used as a binary catalyst with the concentration of 0.1 wt.% each [39]. The Co/Mo catalyst was initially reduced under Ar containing 3%H₂ atmosphere. After the temperature has reached 800°C, 40 μL of pure ethanol (EtOH) were firstly introduced into the CVD chamber, and the first stage of the CVD reaction was kept for 1.30 min at a pressure of about 1.4 to 2.3 kPa. Prior to introduction of 10% mixed acetonitrile ethanol feedstock (10% AcN), the CVD chamber was evacuated to the background pressure of 14 Pa with the dwell time of 30 sec. 40 μL of 10% AcN feedstock were then released into the chamber. N-doped SWNT arrays were continuously grown for another 2.30 min. The CVD chamber was finally cooled down to room temperature. Double layered samples obtained by this procedure are hereafter referred to as SWNT_{Et-Ac}. Samples consisting of only one single layer grown from one feedstock are labeled SWNT_{Et} and SWNT_{Ac}, respectively.

The morphology of VA-SWNT arrays was investigated by scanning electron microscopy (SEM, 1 kV acceleration voltage, S-4800, Hitachi Co., Ltd.). As-grown VA-SWNT arrays were characterized by resonance Raman spectroscopy (Chromex 501is with Andor DV401-FI) using an excitation wavelength of 488 nm. The incident laser with a power of 0.25 mW was focused by a 50× objective lens. For cross sectional Raman measurements the polarization was kept perpendicular to the nanotube axis. For photoelectron spectroscopy (XPS), VA-SWNT arrays were firstly heated at 400°C in vacuum (14 Pa) to dehydrate and desorb N₂ molecules before the measurement. The XPS spectra were measured with a PHI 5000 VersaProbe setup with 1.486 keV. For control experiments, SWNT_{Ac} and SWNT_{Et} were annealed in air at 500°C for 10 min to remove the nanotube cap [40] and release the encapsulated N₂ molecules

3.2) Application on solar cells

- Synthesis of single-walled carbon nanotubes (SWNTs)

SWNTs were synthesized at 800 °C by alcohol-catalytic chemical vapor deposition (CVD) process [11]. The cobalt acetate (Co) and iron nitrate (Fe) used as binary catalyst were prepared by impregnation method with zeolite particles. The concentration of 2.5 wt.% each of Co and Fe were dissolved in 40 g of ethanol along with 1 g of zeolite particles. The solution was then mild sonicated for 90 min before leaving it dried at 80°C. Dried catalytic zeolite was ground, and catalytic powder of Co/Fe binary catalyst was stored at 80°C for use in nanotube synthesis.

A quartz boat containing the catalytic powder was placed in the CVD furnace and heated to 800°C under 3%H₂ atmosphere to reduce catalysts for 30 min. Once the growth temperature was reached, the Ar/H₂ supply was terminated. Ethanol vapor was then flowed into the CVD chamber with a flow rate of 450 sccm for 10 min, prior to cooling down to room temperature.

Preparation of nanotube film

SWNT film was prepared based on the process reported in [41]. As-grown SWNTs on zeolite particles were dispersed in deionized water containing 1% of sodium dodecylbenzenesulfonate (SDBS) surfactant. Dispersed SWNTs were mild sonicated for 90 min and ultra-sonicated for 30 min. The nanotube suspension was then centrifuged for 15 min at the speed of 85,000 rpm (327,000g). Eventually, the supernatant was extracted. In order to make the nanotube film, the supernatant was filtered by vacuum filtration process and rinsed again with deionized water. The supernatant was also used for further optical measurements. The nanotube film was finally obtained by dissolving filtration membrane with acetone and rinsed again with isopropyl alcohol.

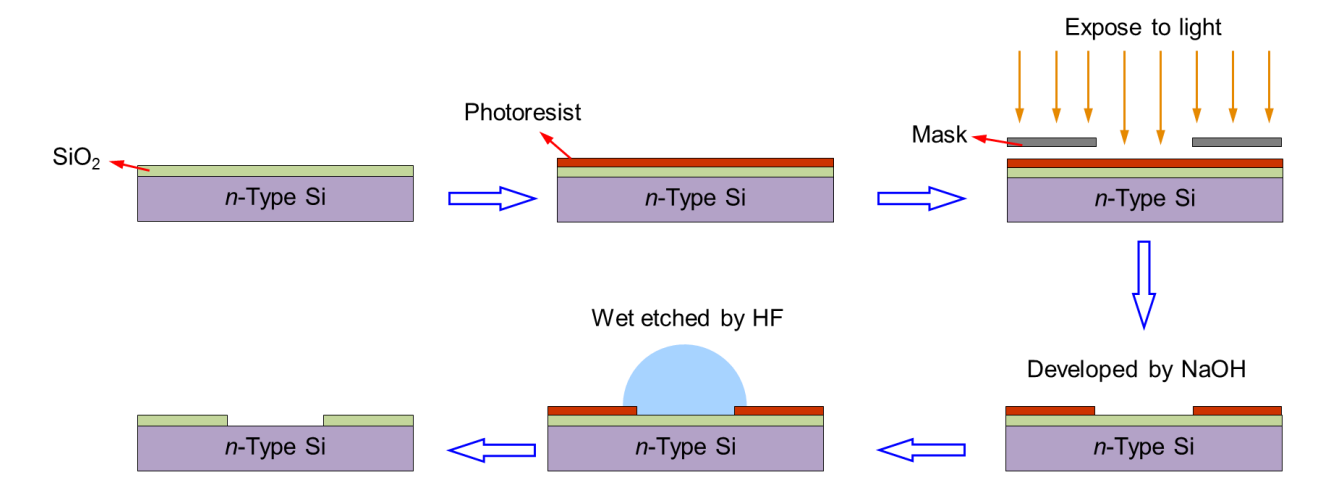


Fig. 1 Schematic of silicon substrate pattering by wet-etching and photolithography processes.

- Solar-cells fabrication

Heterojunction solar cell was fabricated from *n*-type silicon and SWNT film. Patterned silicon was made by photolithography process. Photoresist was spin-coated on silicon wafer, and heated at 90°C for 5 min. The wafer was patterned by light passing through physical mask with the window size of 0.3 cm×0.3 cm for 1 h (Fig. 1), prior to developing in NaOH solution (14%) for 1 min. Hydrofuric acid (HF) with concentration of 20% was used to etch SiO₂ layer by dropping on exposed area. The rest of photoresist was dissolved in acetone, and the etched SiO₂ layer was rinsed with isopropyl alcohol before baking at 120°C for 5 min. Gold (Au) with the thickness of 40 nm was then evaporated on top of the SiO₂ layer and on the backside of silicon wafer to serve as electrodes. The prepared SWNT film was finally transferred onto the patterned *n*-type silicon.

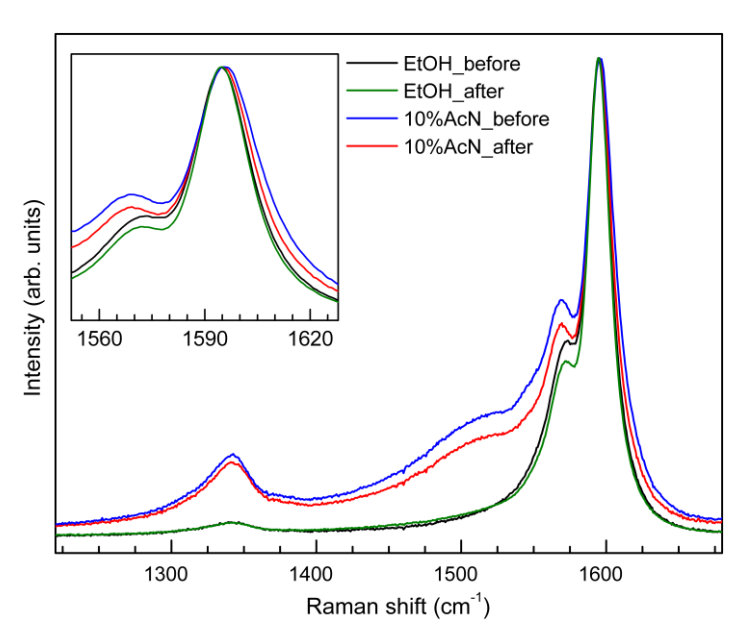


Fig. 2 A comparison of resonance Raman spectra of SWNTs synthesized from ethanol (EtOH) and 10% acetonitrile (10% AcN) before and after annealing at 500°C for 10 min.

4. Result and Discussions

4.1) Synthesis of N-doped SWNT and double-layered growth

Signatures of encapsulated N₂

Fig. 2 shows the comparison of G-band linewidth before and after annealing of SWNT_{Et} and SWNT_{Ac}. The G-Band is observed at 1594 cm⁻¹. The prominent Breit-Wigner-Fano (BWF) lineshape and higher D-band intensity is at this wavelength a distinct feature of SWNT_{Ac}, thus they can be distinguished from SWNT_{Et}. The G-bands were fitted using one fixed Fano lineshape at 1571 cm⁻¹, one fixed Lorentzian peak at 1607 cm⁻¹, and one free Lorentzian peak for EtOH case, as well as, one fixed Fano lineshape at 1521 cm⁻¹, five fixed Lorentzian peaks at 1486, 1552, 1568, 1607 cm⁻¹, and one free Lorentzian peak for 10% AcN case. The G-band linewidth of SWNT_{Ac} sharpens after annealing in air, while its frequency is unchanged, its full width at half maximum (FWHM) is narrower by approximately 1.1 cm⁻¹. This constriction of the G-band linewidth indicates the disappearance of the harmonic coupling of trapped N₂ molecules and carbon atoms in the nanotubes. Consistently, there is no such change in the G-band linewidth for SWNT_{Et}.

The Raman data points at encapsulated N_2 molecules specifically inside not-annealed 10% AcN-grown SWNTs, interacting with the host and shortening the phonon life-times [42]. The carbon structures forming a nanotube cap are readily removed by annealing at 500°C, due to their increased reactivity [40,43]. The control experiment also demonstrates that encapsulated N_2 are mobile and can reach the open end due to weak bonding with graphitic carbon walls as observed in multi-walled carbon nanotubes [44].

The presence of N_2 molecules was also directly detected by XPS measurements. Fig. 3 shows a comparison of XPS spectra of SWNT Ac before and after annealing. The well-defined asymmetric Doniach-Sunjic lineshape of the C1s peaks at 284.6 eV with π - π * electron shake up is a common feature of SWNTs [26,34]. The binding energy at about 404 eV identifies N_2 molecules inside N-doped SWNT hosts [45]. The N content was evaluated using relative XPS peak areas with the relative atomic cross section of 1.8 for N/C [46]. The abundance of N_2 molecules was found to be approximately 0.3 at.% in pristine SWNT_{Ac}, while the signal of N after annealing is well within the noise level. The disappearance of the N_2 signal at the binding energy of 404 eV after opening the cap by annealing is consistent with the Raman data and confirms the escape of N_2 from the interior of SWNTs. The easy removal of linear arrangements of N_2 inside SWNTs is strongly contrasted by gas molecules trapped inside more complex crystal structures, where the escape path is sterically blocked [47]. Note that the observed binding energy of encapsulated N_2 molecules is lower than that of free molecular gaseous N_2 (409.9 eV) [48]. This can be explained by electron screening for N1s core-holes due to surrounding cylinder of sp^2 carbon [49].

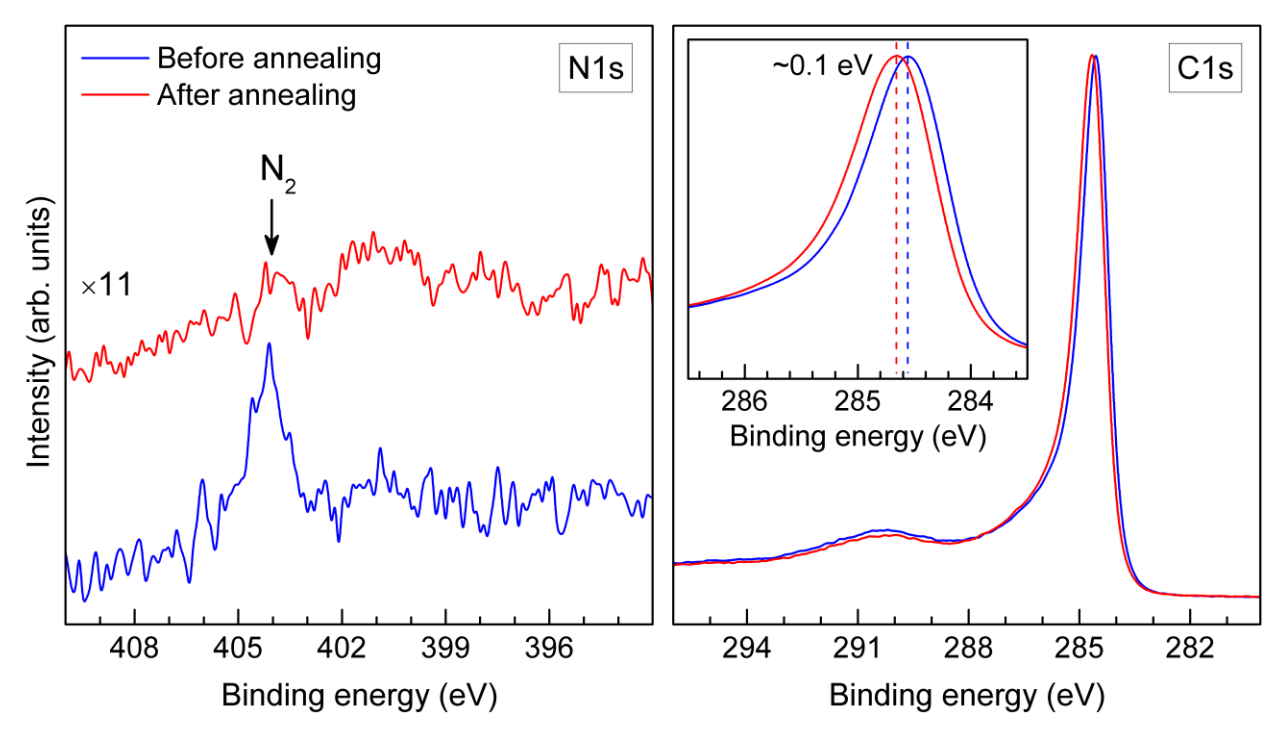


Fig. 3 Photoemission spectra of N-doped SWNT films synthesized from 10% acetonitrile feedstock mixture in ethanol before and after annealing in air at 500°C. The disappearance of N₂ signal was observed after annealing.

Additionally, a shift in the C1s peak of approximately 0.1 eV without broadening (Fig. 3) was observed. While the hosting SWNT walls can provide the dielectric environment for screening the N1s core level in the encapsulated N₂, the reverse mechanism cannot occur. 0.3 at.% of N cannot affect the macroscopic average screening of the C1s core-hole excitation. We argue that this shift is rather due to the different C1s binding energies in metallic and semiconducting SWNTs [50], and the fact that small diameter metallic SWNTs are also more susceptible to oxidation. This interpretation is also in line with the reduced strength of the Fano component in the G-line in annealed SWNTs as shown in Fig. 2.

- Migration of N₂ molecules

Two differently stacked SWNT arrays from EtOH and 10% AcN grown SWNTs were synthesized by introducing the two carbon feedstocks in sequence. Fig. 4 shows the interface between the layers obtained at the successive stages of the growth, and shows interconnectivity at the length scale of SWNT bundles. The interface is highlighted by yellow arrows. Starting with EtOH feedstock, the initial growth of SWNTs was observed with a thickness of about 5 μ m, whereas 6.5 μ m of the bottom layer are grown from 10% AcN. The visible interface between the layers are interpreted as recorded changes in growth rates and feedstock flux. Note that the actual growth was

halted for 30 s. Similar horizontal bands were observed in incremental growth with pulsed carbon flux [51].

The cross sectional Raman spectra of layered samples clearly demonstrate spectral features of SWNT_{Ac} and SWNT_{Et} [52] in the corresponding layers. The feedstock sequence and layer sequence do match the root growth mechanism [38]. As shown in our earlier report [52], the small-diameter RBM peaks in the range of 100-400 cm⁻¹ are predominant for N-doped SWNTs. Fig. 5 shows the comparison of resonance Raman spectra of SWNT arrays synthesized from pure EtOH and SWNT_{Et-Ac} array. The top surface of the films was measured in both cases.

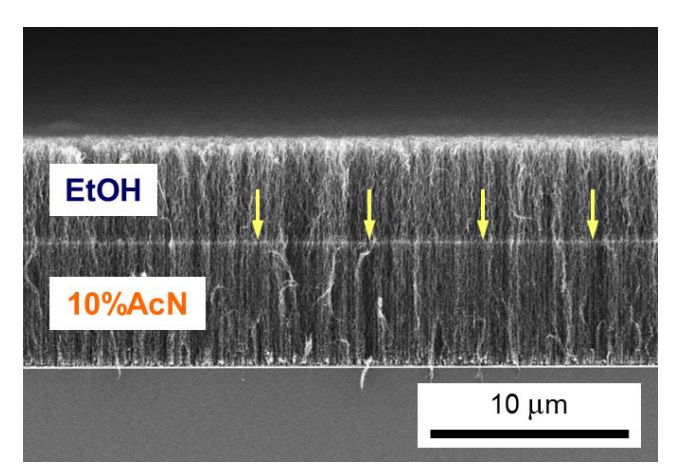


Fig. 4 SEM micrographs of double-layered N-doped SWNT array synthesized from ethanol (EtOH) and 10% acetonitrile feedstock mixture in ethanol (10% AcN), respectively. Yellow arrows highlight the interface between different SWNT arrays at which the feedstock was switched.

The RBM peaks at 145 and 180 cm $^{-1}$ at 488 nm excitation are a well known feature for vertical aligned arrays [53]. The broadening of the G-band linewidth in SWNT_{Et-Ac} array can be seen in the inset in Fig. 5. It suggests that there are, like in the case of SWNT_{Ac}, N₂ molecules trapped inside the top layer of SWNT_{Et-Ac} [42].

XPS measurements were performed on the top surface of SWNT Et-Ac as shown in Fig. 6, to demonstrate the presence of diatomic N_2 molecules in the top layer of double-layered SWNT array where the nanotubes were initially grown from EtOH. The survey scan in the inset shows the strong C1s core level of carbon with absent O_2 absorption after sample annealing.

The signatures of trapped N_2 molecules inside EtOH-grown SWNTs (top layer) is confirmed by the notable peak at the binding energy of 404 eV. This proves the migration of N_2 molecules from the bottom (10%AcN) layer to the top (EtOH) layer. Note that a 5 μ m thickness of the top layer is far beyond the escape depth of photoelectrons in dense and homogeneous SWNT arrays. The signal from diatomic N_2 is therefore not attributed to the interface region where the feedstock was switched from EtOH to 10%AcN, or even the bottom layer.

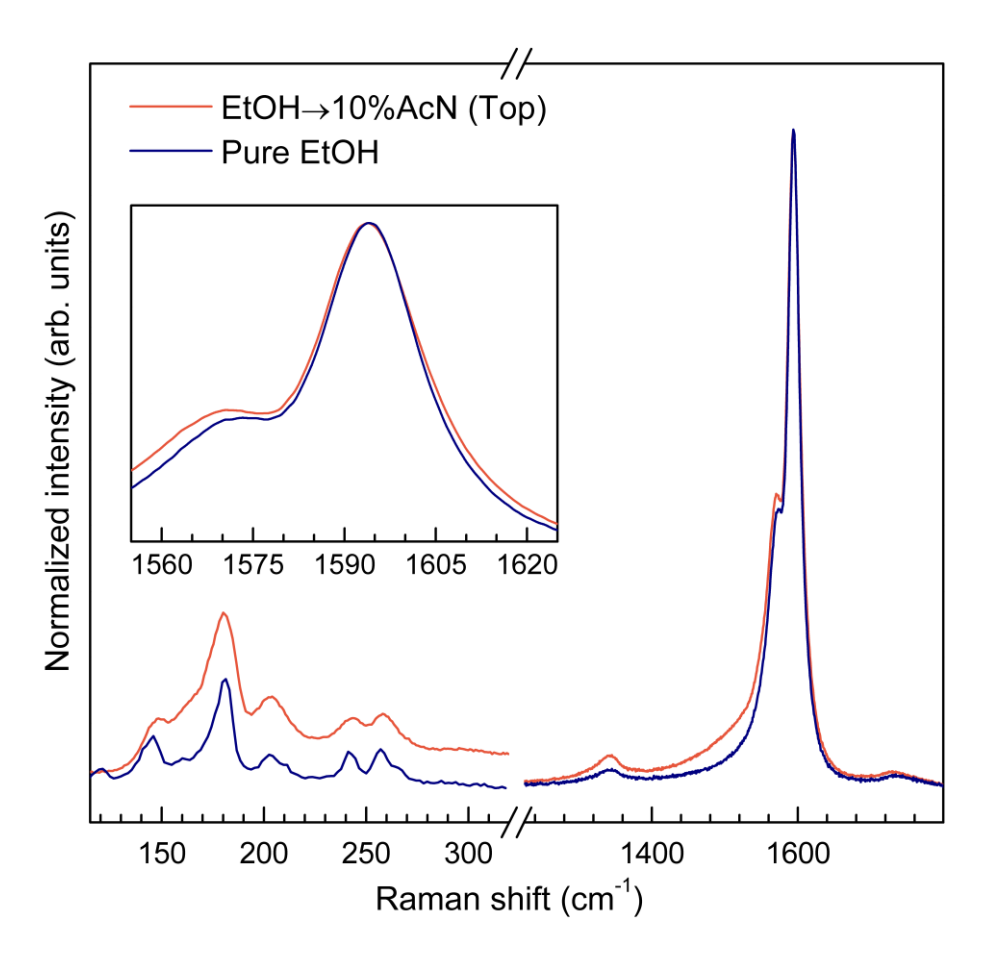


Fig. 5 Raman spectra of a single layered array of SWNT_{EtOH} and a layer of SWNT_{EtOH} with a subsequent layer of SWNT_{Et-Ac} underneath. The excitation wavelength was 488 nm.

The N content in form of N₂ molecules in the top layer is found to be approximately 0.07 at.% (compare to 0.3 at.% in SWNT_{Ac}). This data represents a bulk signature of continuous SWNT throughout a macroscopic sample. In a first approximation disregarding different diameters as well as differences in the thickness of the layers, one would expect to observe about half of the atomic N concentration in double layered SWNT_{Et-Ac}, if all SWNT were running continuously from the bottom of the bottom layer all the way to the top of the top layer. By reversing this estimate we conclude that the fractions of discontinued and continuous SWNT throughout the layers and across the interface are of the same magnitude. Considering that the growth is halted for 30 s during the exchange of feedstocks which should be expected to favor discontinued SWNTs, we have demonstrated that SWNTs in VA-SWNTs diameter controlled CVD growth can yield bulk material of continuous SWNT featuring intramolecular junctions.

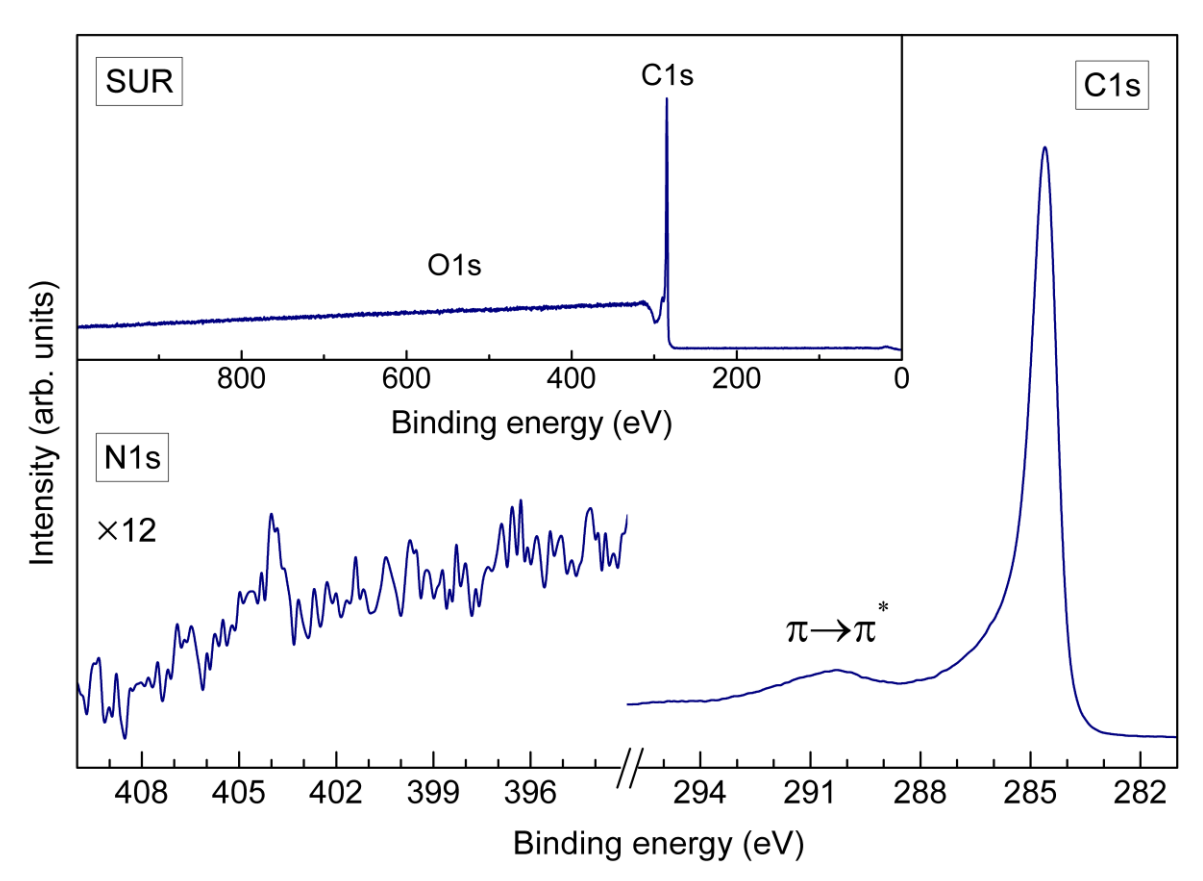


Fig. 6 XPS spectra performed on the top of vertically aligned double-layered SWNT array synthesized from EtOH and 10% AcN, respectively. The molecular N₂ N1s core level is visible. The inset shows the survey scan, indicating very clean sample.

4.2) Application on solar cells

The SEM micrograph in Fig. 7 clearly shows viability of as-grown carbon nanotubes on zeolite particles. SWNTs are demonstrated by Raman spectroscopy with three different excitation wavelengths (488, 514 and 633 nm) as shown in Fig. 8 [54]. The peak at 1594 cm⁻¹ indicates the vibration mode of carbon atom along the axial direction of carbon nanotubes, called tangential mode, or G-band. The splitting of G-band into G⁺ and G⁻ indicate vibration in longitudinal and circumferential directions of carbon atoms. The presence of the so-called RBM mode (100-400 cm⁻¹) implies the vibration of carbon atoms in radial direction. The G-band and RBM indicate that single-walled carbon nanotubes were obtained from ACCVD process. According to correlation, $\omega_{RBM} \approx 217.8/d + 15.7$ [55], the Raman shift of RBM mode (ω_{RBM}) is the inverse of nanotube diameter (d). Certain different nanotube diameters would give rise to specific resonance window with three different excitation energies in RBM region as seen in Fig. 8, and nanotube diameter can be evaluated to be approximately 0.8 to 1.6 nm. The G/D ratio measured by excitation wavelengths of 488, 514 and 633 nm are 12, 19 and 9.4, respectively, indicating less imperfection of carbon lattice and low impurity level in the nanotube sample [54].

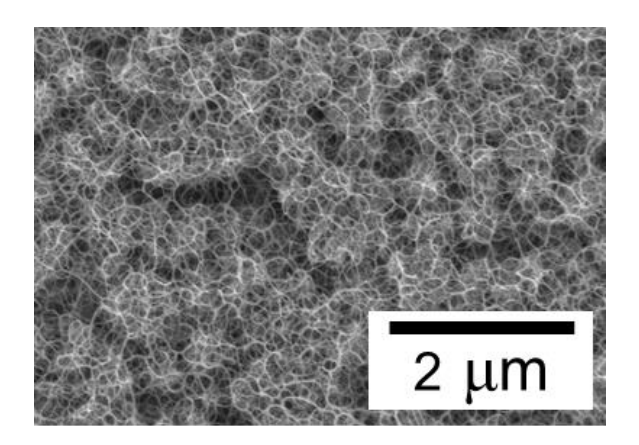


Fig. 7 SEM micrograph of as-grown SWCNTs synthesized from alcohol-catalytic CVD (ACCVD) method on zeolite particles.

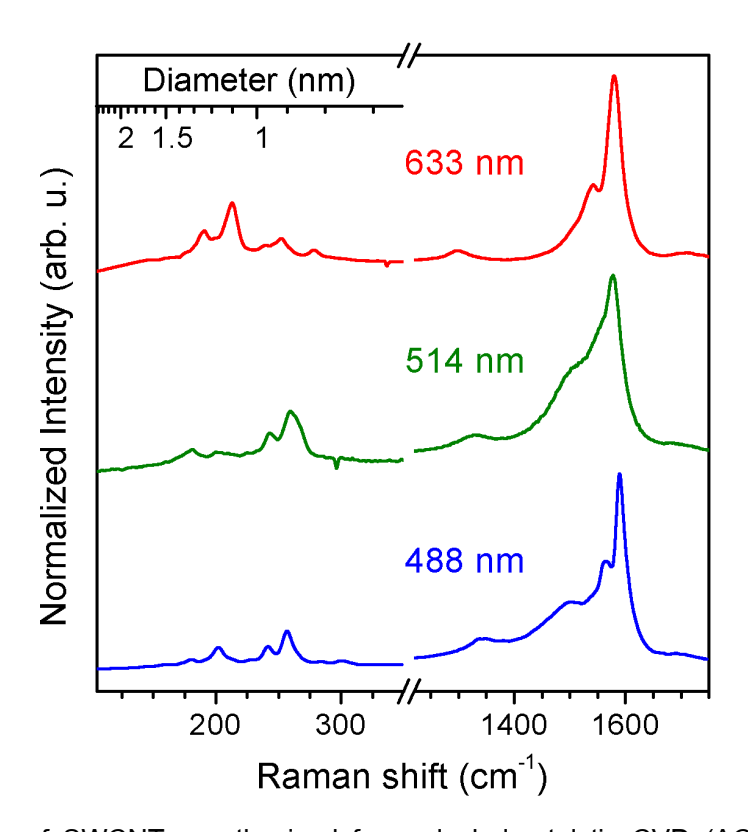


Fig. 8 Raman spectra of SWCNTs synthesized from alcohol-catalytic CVD (ACCVD) method zeolite particles, excited by 488, 514 and 633 nm wavelengths.

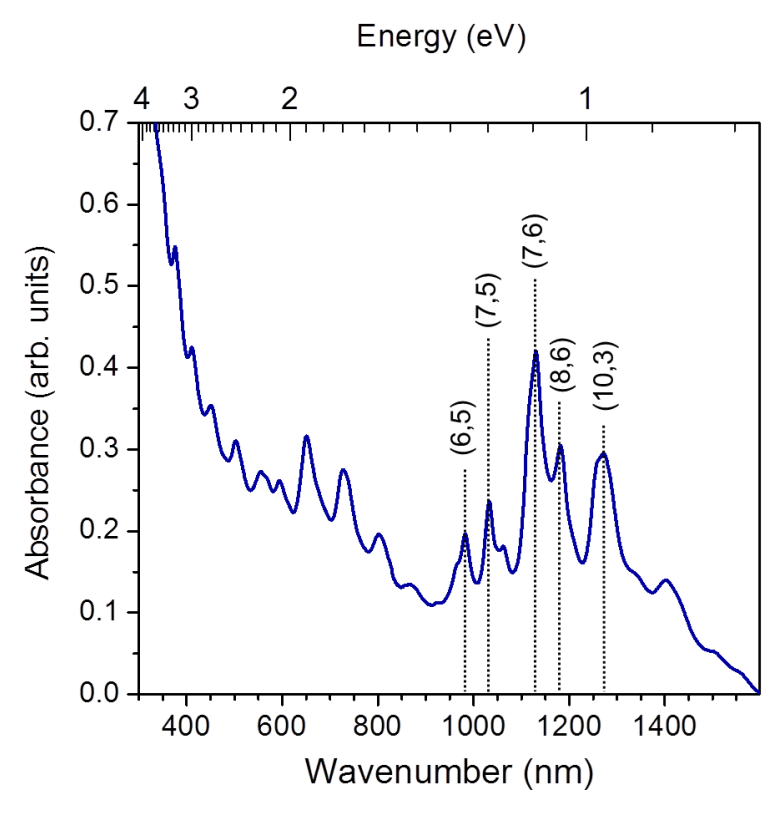


Fig. 9 Optical absorption spectrum of dispersed SWCNTs, revealing the first (S_{11}) and second (S_{22}) electronic transitions of semiconducting nanotubes, and specific chiralities of nanotubes.

Fig. 9 shows the optical absorption spectrum of dispersed SWNTs in water. It reveals the band energy of the first (S_{11}) and second (S_{22}) electronic transitions of semiconducting nanotubes, indicating specific structure of the nanotubes [55]. The S_{11} and S_{22} regions are approximately in the range of 900 to 1500 nm, and 500 to 900 nm, respectively. Specific chiralities are assigned to be (6,5), (7,5), (7,6), (8,6) and (10,3) nanotubes. Based on observable chiralities presented in optical absorbance, nanotube diameter is approximately less than 1 nm [55]. Although the nanotube diameter can be evaluated from the peak positions of S_{11} transition measured from dispersed sample, it does not represent the diameter of the entire sample. TEM measurement was employed for further diameter evaluation (Fig. 10). Fig. 10 shows TEM images of as-grown SWNT dispersed on TEM microgrid, indicating clean single-walled carbon nanotubes. Diameter distribution obtained from 100 nanotubes was shown in the histrogram from TEM observation. The observed mean diameter is about 1.06 \pm 0.24 nm, which corresponds to that obtained from Raman measurement.

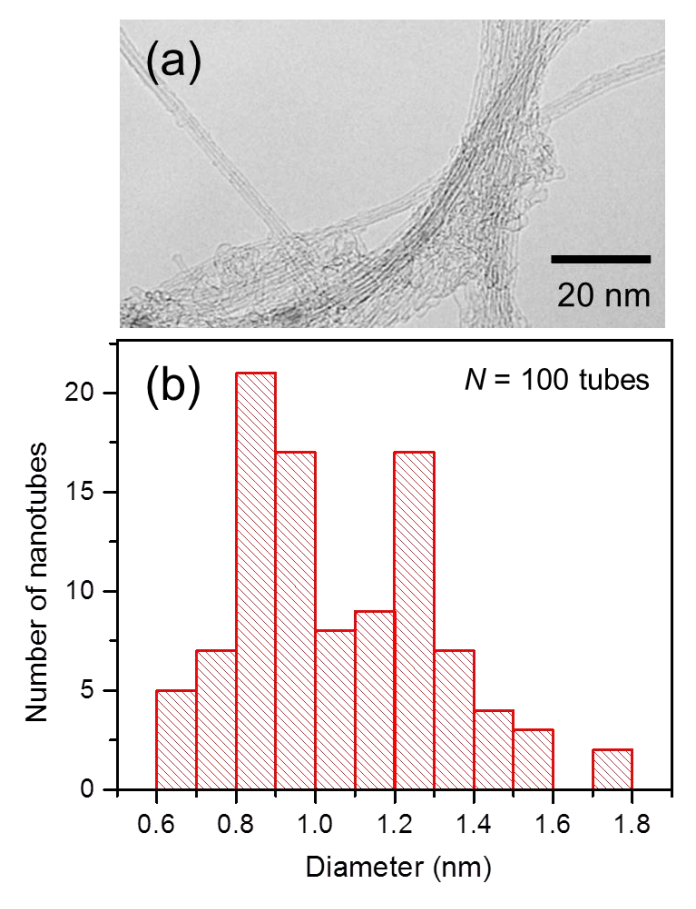


Fig. 10 (a) TEM micrograph of dispersed as-grown SWCNTs, and (b) diameter distribution of nanotube diameter obtained from TEM observation (N = 100 tubes). The observed mean diameter is about 1.06 \pm 0.24 nm.

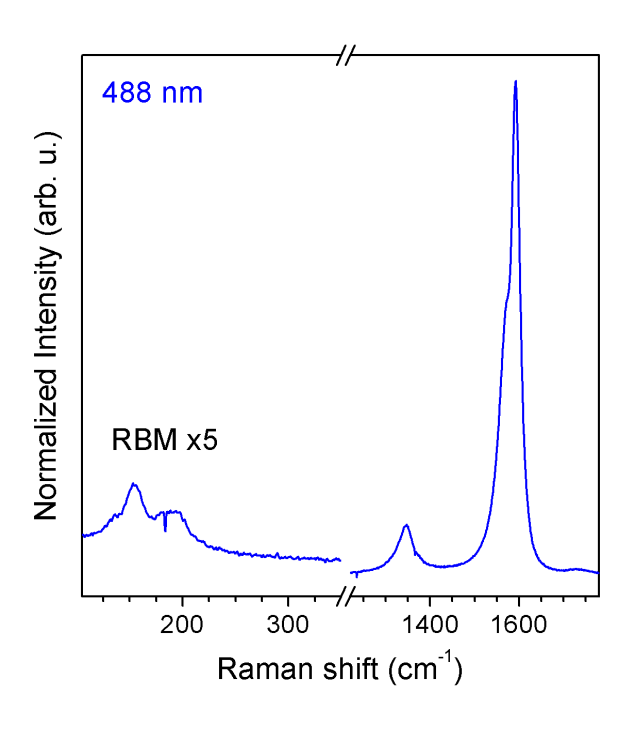


Fig. 11 Raman spectra of as-grown and SWCNT film excited by 488 nm wavelengths, indicating a broadening of G and RBM peaks.

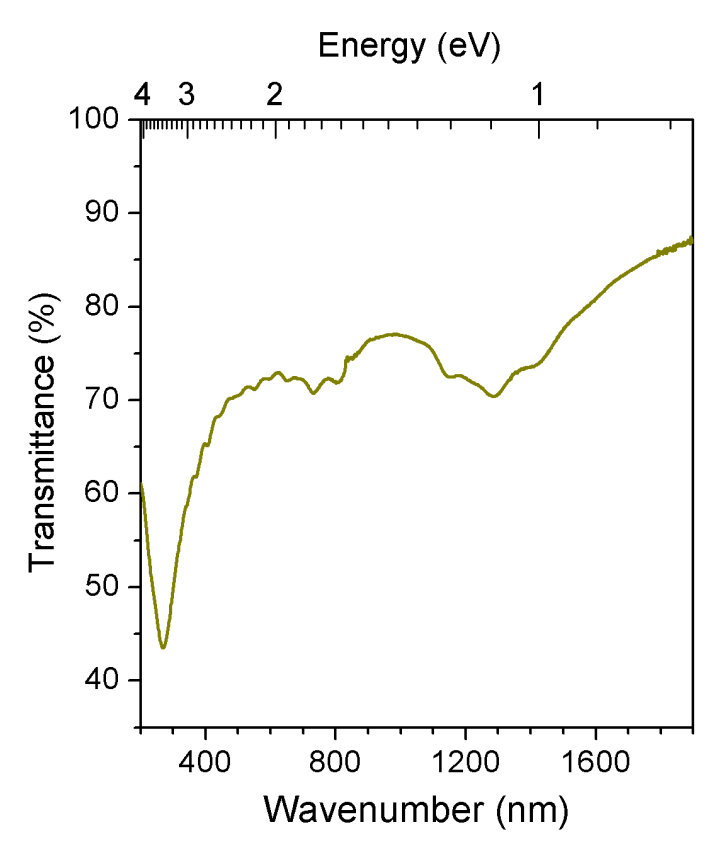


Fig. 12 Transmittance of SWCNT film made from vacuum filtration process.

While Raman peaks obtained from as-grown nanotube sample can be clearly seen, they are more broadened when nanotubes were made into a film due to accumulation of nanotube bundles from the vacuum filtration process (Fig. 11) that may cause change in vibration mode of carbon atoms, resulting in diminishing of peak intensity and peak broadening. Considering the S_{11} transition, transmittance of obtained nanotube film was measured to be about 70% from optical measurement (Fig. 12), and the inset shows SEM micrograph of a uniform nanotube film obtained from vacuum filtration method.

Heterojunction solar cells was fabricated from nanotube film and *n*-type silicon wafer (Fig. 13, inset). The current density-voltage (*J-V*) characteristic of device was obtained under 100 mA/cm² AM1.5G illumination and dark conditions as shown in Fig. 12. The power-conversion efficiency (PCE) and fill factor (FF) were characterized according to the relation [56],

$$\eta = \frac{V_{oc}I_{sc}FF}{P_{in}}$$
, and $FF = \frac{P_{max}}{V_{oc}I_{sc}}$.

when η is PCE value, V_{oc} , I_{sc} are open circuit voltage, respectively, and P_{in} , P_{max} are input and maximum power, respectively. The PCE value of 4.3% was obtained from *J-V* characteristic, while V_{oc} value was 0.52 V and I_{sc} value was 12.18 mA/cm 2 . In addition to PCE value, The FF is an important factor used to indicate solar cell performance. It represents the rectangularity of the *I-V*

curve, and can be obtained from the defined maximum power divided by the product of $I_{sc}V_{oc}$. In Fig. 13, the FF obtained from the maximum power of 4.3 mW/cm 2 was evaluated to be 0.67. The photocurrent generation mechanism of SWNT-silicon heterojunction can be considered as p-n heterojunction [57,58]. Nanotube film serves as hole collector, and meanwhile random cross-linked nanotube bundle could also act as conduction pathway from tube to tube, resulting in good efficiency and fill factor. However, the presence of electron-hole recombination may imply the limitation in the FF and PCE values for silicon heterojunction solar cells [59], unlike values obtained from previous reports [60,61] in which polymer layers were served as barrier to reduce reflectance of the surface along with carrier modifications. Likewise, it may be plausible that the recombination can be reduced by controlling the thickness of oxide layer during wet-etching process to serve as electron-hole barrier [62], which will be investigated further in order to achieve better improvement of nanotube-heterojunction solar cell performance.

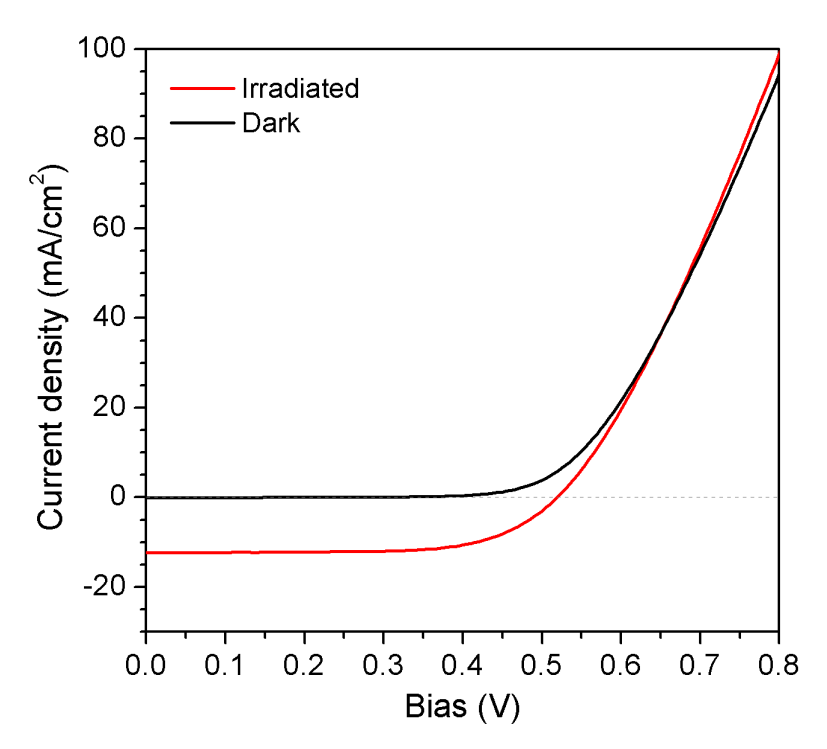


Fig. 13 J-V characteristics of SWCNT solar cells measured under AM1.5G 100 mW/cm².

5. Conclusion

5.1) Synthesis of N-doped SWNT and double-layered growth

The Raman and XPS signatures of encapsulated nitrogen molecules inside N-doped SWNTs were presented. The nanotube cap could be opened by annealing in air to release the trapped molecules. The presence of and disappearance of N_2 were detected by photoemission. The Raman spectra reveal a characteristic broadening and sharpening of the G-band, with the presence and

removal of N_2 . The XPS data shows in the lowered N1s binding energy the effect of the surrounding matrix on the encapsulated N_2 , while Raman spectroscopy probes the effect of the encapsulated N_2 on the hosting SWNT. Both effects change consistently upon release of the N_2 and conclusively evidence the migration of N_2 molecules inside continuous SWNTs in double-layered samples. The G-line phonon lifetime in the top layer grown from pure EtOH is notably increased and a relative atomic N concentration of ~1/4 allows to conclude that there are comparable fractions of continuous and discontinued SWNTs across the interface of diameter controlled layers of VA-SWNTs.

5.2) Application on solar cells

We have achieved a simple fabrication of heterojunction solar cells from single-walled carbon nanotubes (SWNTs) and *n*-type silicon wafer. The patterned silicon substrate was prepared via a simple wet-etching process by dropping hydrofuric acid over a hand-made physical mask. Power-conversion efficiency value of 4.3% and fill factor of 0.67 are obtained from the nanotube film with the mean nanotube diameter of about 1.1 nm without any post-treatment process, while the transparency of the nanotube film prepared by vacuum filtration is 70%. In future work, the fabrication of heterojunction solar cells using other types of nanomaterials could be explored along with possibility of fabricating flexible solar cells with thin film silicon. A simple fabrication of heterojunction solar cells by wet-etching process could be performed with good power-conversion efficiency, although silicon is employed in the process. The use of wet-etching process has given potential for future research and development.

Reference:

- 1. B. Kitiyanan, W. E. Alvarez, J. H. Harwell, and D. E. Resasco, *Chem. Phys. Lett.* 317, 497 (2000).
- S. Bandow, S. Asaka, Y. Saito, A. M. Rao, L. Grigorian, E. Richter, and P. C. Eklund, *Phys. Rev. Lett.* 80, 3779 (1998).
- 3. W.-H. Chiang and R. M. Sankaran, Nat. Mater. 8, 882 (2009).
- 4. R. Xiang, E. Einarsson, Y. Murakami, J. Shiomi, S. Chiashi, Z. Tang, and S. Maruyama, *ACS Nano* **6**, 7472 (2012).
- S. M. Bachilo, L. Balzano, J. E. Herrera, F. Pompeo, D. E. Resasco, and R. B. Weisman, *J. Am. Chem. Soc.* 125, 11186 (2003).
- 6. Y. Miyauchi, S. Chiashi, Y. Murakami, Y. Hayashida, and S. Maruyama, *Chem. Phys. Lett.* **387**, 198 (2004).
- 7. H. Kataura, Y. Kumazawa, Y. Maniwa, Y. Ohtsuka, R. Sen, S. Suzuki, and Y. Achiba, *Carbon* 38, 1691 (2000).

- 8. L. An, J. M. Owens, L. E. McNeil, and J. Liu, J. Am. Chem. Soc. 124, 13688 (2002).
- 9. A. G. Nasibulin, P. V. Pikhitsa, H. Jiang, and E. I. Kauppinen, Carbon 43, 2251 (2005).
- B. Wang, C. H. P. Poa, L. Wei, L.-J. Li, Y. Yang, and Y. Chen, *J. Am. Chem. Soc.* 129, 9014 (2007).
- 11. Y. Murakami, Y. Miyauchi, S. Chiashi, and S. Maruyama, Chem. Phys. Lett. 374, 53 (2003).
- H. Ago, S. Imamura, T. Okazaki, T. Saito, M. Yumura, and M. Tsuji, *J. Phys. Chem. B* **109**, 10035 (2005).
- 13. D. Ciuparu, Y. Chen, S. Lim, G. L. Haller, and L. Pfefferle, J. Phys. Chem. B 108, 503 (2004).
- 14. A. M. Rao, P. C. Eklund, S. Bandow, A. Thess, and R. E. Smalley, Nature 388, 257 (1997).
- 15. C. Zhou, J. Kong, E. Yenilmez, and H. Dai, Science 290, 1552 (2000).
- 16. M. Bockrath, J. Hone, A. Zettl, P. L. McEuen, A. G. Rinzler, and R. E. Smalley, *Phys. Rev. B* **61**, R10606 (2000).
- 17. D. Golberg, Y. Bando, L. Bourgeois, K. Kurashima, and T. Sato, Carbon 38, 2017 (2000).
- 18. U. Bangert, A. Bleloch, M. H. Gass, A. Seepujak, and J. van den Berg, *Phys. Rev. B* **81**, 245423 (2010).
- 19. F. Xu, M. Minniti, C. Giallombardo, A. Cupolillo, P. Barone, A. Oliva, and L. Papagno, *Surf. Sci.* **601**, 2819 (2007).
- 20. P. G. Collins, K. Bradley, M. Ishigami, A. Zettl, Science 287, 1801 (2000).
- R. Droppa, C. T. M. Ribeiro, A. R. Zanatta, M. C. dos Santos, and F. Alvarez, *Phys. Rev. B* 69, 045405 (2004).
- 22. H. C. Choi, J. Park, and B. Kim, J. Phys. Chem. B 109, 4333 (2005).
- L. H. Chan, K. H. Hong, D. Q. Xiao, T. C. Lin, S. H. Lai, W. J. Hsieh, and H. C. Shih, *Phys. Rev. B* 70, 125408 (2004).
- 24. S. Maldonado, S. Morin, and K. J. Stevenson, Carbon 44, 1429 (2006).
- 25. A. A. Koós, M. Dowling, K. Jurkschat, A. Crossley, and N. Grobert, Carbon 47, 30 (2009).
- P. Ayala, A. Grüeis, T. Gemming, D. Grimm, C. Kramberger, M. H. Rümmeli, F. L. Freire, H. Kuzmany, R. Pfeiffer, A. Barreiro, B. Büchner, and T. Pichler, J. Phys. Chem. C 111, 2879 (2007).
- 27. P. Ayala, A. Grüneis, T. Gemming, B. Büchner, M. H. Rümmeli, D. Grimm, J. Schumann, R. Kaltofen, F. L. Freire Jr., H. D. F. Filho, and T. Pichler, *Chem. Mater.* 19, 6131 (2007).
- 28. H. Lin, R. Arenal, S. Enouz-Vedrenne, O. Stephan, and A. Loiseau, *J. Phys. Chem. C* 113, 9509 (2009).
- H. Lin, J. Lagoute, C. Chacon, R. Arenal, O. Stéphan, V. Repain, Y. Girard, S. Enouz, L. Bresson, S. Rousset, and A. Loiseau, *Phys. Status Solidi B* 245, 1986 (2008).

- F. Villalpando-Paez, A. Zamudio, A. Elias, H. Son, E. Barros, S. Chou, Y. Kim, H. Muramatsu, T. Hayashi, J. Kong, H. Terrones, G. Dresselhaus, M. Endo, M. Terrones, and M. Dresselhaus, Chem. Phys. Lett. 424, 345 (2006).
- 31. Z. Zhu, H. Jiang, T. Susi, A. G. Nasibulin, and E. I. Kauppinen, *J. Am. Chem. Soc.* **133**, 1224 (2011).
- 32. S.-G. KIM, S.-Y. KIM, and H.-W. LEE, *Trans. Nonferrous Met. Soc. China* 21, Supplement 1, s130 (2011).
- 33. P. Ayala, A. Grüneis, C. Kramberger, M. H. Rümmeli, I. G. Solorzano, J. Freire, F. L., and T. Pichler, *J. Chem. Phys.* **127**, 184709 (2007).
- 34. E. Ibrahim, V. O. Khavrus, A. Leonhardt, S. Hampel, S. Oswald, M. H. Rümmeli, and B. Büchner, *Diamond Relat. Mater.* **19**, 1199 (2010).
- 35. A. R. Rocha, M. Rossi, A. J. R. da Silva, and A. Fazzio, *J. Phys. D: Appl. Phys.* **43**, 374002 (2010).
- 36. D. Usachov, O. Vilkov, A. Grüneis, D. Haberer, A. Fedorov, V. K. Adamchuk, A. B. Preobrajenski, P. Dudin, A. Barinov, M. Oehzelt, C. Laubschat, and D. V. Vyalikh, *Nano Lett.* **11**, 5401 (2011).
- T. Schiros, D. Nordlund, L. Pálová, D. Prezzi, L. Zhao, K. S. Kim, U. Wurstbauer, C. Gutiérrez, D. Delongchamp, C. Jaye, D. Fischer, H. Ogasawara, L. G. M. Pettersson, D. R. Reichman, P. Kim, M. S. Hybertsen, and A. N. Pasupathy, *Nano Lett.* 12, 4025 (2012).
- 38. R. Xiang, Z. Zhang, K. Ogura, J. Okawa, E. Einarsson, Y. Miyauchi, J. Shiomi and S. Maruyama, *Jpn. J. Appl. Phys.* 47, 1971 (2088).
- 39. Y. Murakami, Y. Miyauchi, S. Chiashi and S. Maruyama, Chem. Phys. Lett. 377, 49 (2003).
- 40. P. M. Ajayan, T. W. Ebbesen, T. Ichihashi, S. Iijima, K. Tanigaki and H. Hiura, *Nature* **362**, 522 (1993).
- 41. Z. Wu, Z. Chen, X. Du, J.M. Logan, J. Sippel, M. Nikolou, K. Kamaras, J.R. Reynolds, D.B. Tanner, A.F. Hebard and A.G. Rinzler, *Science* **305**, 1273 (2004).
- 42. S. Gayen, S. N. Behera and S. M. Bose, Phys. Rev. B 76, 165433 (2007).
- 43. P. M. Ajayan and S. lijima, *Nature* 361, 333 (1993).
- 44. H. C. Choi, S. Y. Bae, W.-S. Jang, J. Park, H. J. Song, H.-J. Shin, H. Jung and J.-P. Ahn, *J. Phys. Chem. B* **109**, 1683 (2005).
- 45. C. Kramberger, T. Thurakitseree, H. Koh, Y. Izumi, T. Kinoshita, T. Muro, E. Einarsson and S. Maruyama, *Carbon* **55**, 196 (2013).
- 46. J. Scofield, J. Electron Spectrosc. Relat. Phenom. 8, 129 (1976).
- 47. W.-T. Chen, Y. Yamada, G.-N. Liu, A. Kubota, T. Ichikawa, Y. Kojima, G.-C. Guo and S. Fukuzumi, *Dalton Trans.* **40**, 12826 (2011).

- 48. C. R. Brundle, J. Vac. Sci. Technol. 13, 301 (1976).
- 49. O. Björneholm, A. Nilsson, A. Sandell, B. Hernnäs and N. Mrtensson, *Phys. Rev. Lett.* **68**, 1892 (1992).
- 50. P. Ayala, Y. Miyata, K. De Blauwe, H. Shiozawa, Y. Feng, K. Yanagi, C. Kramberger, S. R. P. Silva, R. Follath, H. Kataura and T. Pichler, *Phys. Rev. B* **80**, 205427 (2009).
- D. B. Geohegan, A. A. Puretzky, J. J. Jackson, C. M. Rouleau, G. Eres and K. L. More, ACS Nano 5, 8311 (2011).
- 52. T. Thurakitseree, C. Kramberger, A. Kumamoto, S. Chiashi, E. Einarsson and S. Maruyama, *ACS Nano* 7, 2205 (2013).
- 53. Y. Murakami, E. Einarsson, T. Edamura and S. Maruyama, Phys. Rev. Lett. 94, 087402 (2005).
- 54. M.S. Dresselhaus, G. Dresselhaus, R. Saito, A. Jorio, Phys. Rep. 409, 47 (2005).
- 55. P.T. Araujo, S.K. Doorn, S. Kilina, S. Tretiak, E. Einarsson, S. Maruyama, H. Chacham, M.A. Pimenta, A.Jorio, *Phys. Rev. Lett.* **98**, 067401 (2007).
- 56. J. Nelson, The physics of solar cells, Imperial College Press, 2003.
- J. Wei, Y. Jia, Q. Shu, Z. Gu, K. Wang, D. Zhuang, G. Zhang, Z. Wang, J. Luo, A. Cao, D. Wu, Nano Lett. 7, 2317 (2007).
- Y. Jia, J. Wei, K. Wang, A. Cao, Q. Shu, X. Gui, Y. Zhu, D. Zhuang, G. Zhang, B. Ma, L. Wang,
 W. Liu, Z. Wang, J. Luo, D. Wu, *Adv. Mater.* 20, 4594 (2008).
- 59. M. Reusch, M. Bivour, M. Hermle, S.W. Glunz, Energy Procedia 38, 297 (2013).
- 60. L. Yu, D.D. Tune, C.J. Shearer, J.G. Shapter, Sol. Energy 118, 592 (2015).
- X. Li, X. Zang, X. Li, M. Zhu, Q. Chen, K. Wang, M. Zhong, J. Wei, D. Wu, H. Zhu, Adv. Energy Mater. 4, 1400224 (2014).
- 62. D. Tune, J. Shapter, Nanomaterials 3, 655 (2013).

6. Output (Acknowledge the Thailand Research Fund)

6.1 International Journal Publication

- T. Thurakitseree, S. Choopun and P. Singjai, "Simple fabrication of heterojunction solar cells by utilizing carbon materials films", *Surface & Coatings Technology* (2016) 306, 127–131.
- T. Thurakitseree, C. Kramberger, P. Singjai, and S. Maruyama, "Fingerprinting seamless single-walled carbon nanotube junctions via migration of encapsulated N₂ molecules: From bottom to top, are arrays of vertically aligned SWNT continuous?", Nanoscale (2016), submitted.

6.2 Application

This research study has been utilized by Program in Materials science and Applied physics, Faculty of Science, Maejo University, and some other institutes. It is also very useful for Master students, Program in Nanoscience and nanotechnology, especially studies with authentic laboratory leading to student's motivations and interest in nanotechnology.

From the aim of this research, "CVD synthesis, structure control and characterizations of nitrogen-doped single-walled carbon nanotubes for electrical and mechanical applications", diameter and structure control of SWNTs with nitrogen doping could be successfully achieved along with application on photovoltaic devices. According to journal publications, this research can light up the fundamental knowledge, and construct new researchers for nanotechnology field.